

# Analysis of Full Aircraft with Massive Separation using Detached-Eddy Simulation

Kyle D. Squires  
Arizona State University

James R. Forsythe  
United States Air Force Academy

Scott A. Morton, Douglas C. Blake, Matthieu Serrano  
United States Air Force Academy

Ken E. Wurtzler, William Z. Strang, Robert F. Tomaro  
Cobalt Solutions, LLC

Philippe R. Spalart  
Boeing Commercial Airplanes

## Abstract

One of the more substantial challenges facing Computational Fluid Dynamics is accurate prediction of massively separated flows at high Reynolds numbers. In 1997, Spalart *et al.* [1] proposed Detached-Eddy Simulation (DES) with this challenge in mind. The method is hybrid, combining Reynolds-averaged Navier Stokes (RANS) approaches with Large Eddy Simulation (LES). DES capitalizes on the efficiency of RANS methods in the boundary layer and the accuracy of LES in separated regions. LES, and therefore DES, yields a wider range of unsteady flow features as grid densities are increased and requires a time-accurate and three-dimensional numerical solution. The need for time-accurate solutions on dense grids mandates high performance parallel computation in order to enhance DES efforts. The present Challenge project has focused on both fundamental aspects of the technique and practical applications of importance to current DoD needs. To date, numerous flows have been examined, including a cylinder, two- and three-dimensional forebodies, a prolate spheroid, a supersonic base flow, a delta wing, a parachute, the C130, the X-38, the F-16, the F/A-18E, and the F-15E. Summaries of the calculations are presented in this contribution. The computations are performed on structured and unstructured grids using a flow solver – Cobalt – which uses Message Passing Interface (MPI) for parallel solution. Calculations have been performed on a variety of HPC machines. Depending on the problem size, solutions are obtained on as many as 512 processors, providing time-dependent solutions of the flow around full aircraft in approximately one to two days.

# Introduction

Most of the flow fields encountered in DoD applications occur within and around complex devices and at speeds for which the underlying state of the fluid motion is turbulent. While Computational Fluid Dynamics (CFD) is gaining increased prominence as a useful approach to analyze and ultimately design configurations, efficient and accurate solutions require substantial effort and expertise in several areas. Geometry description and grid generation, numerical solution of the Navier-Stokes equations, and efficient post-processing are all key elements.

While advances have taken place in areas such as grid generation and fast algorithms for solution of systems of equations, CFD has remained limited as a reliable tool for prediction of inherently unsteady flows at flight Reynolds numbers. Current engineering approaches to prediction of unsteady flows are based on solution of the Reynolds-averaged Navier-Stokes (RANS) equations. The turbulence models employed in RANS methods necessarily model the entire spectrum of turbulent motions. While often adequate in steady flows with no regions of reversed flow, or possibly exhibiting shallow separations, it appears inevitable that RANS turbulence models are unable to accurately predict phenomena dominating flows characterized by massive separations. The underlying structure of unsteady massively separated flow is dominated by geometry-dependent and three-dimensional turbulent eddies. These eddies, arguably, are what defeats RANS turbulence models, of any complexity.

To overcome the deficiencies of RANS models for predicting massively separated flows, Spalart *et al.* [1] proposed Detached-Eddy Simulation (DES). The objective was to develop a numerically feasible and accurate approach combining the most favorable elements of RANS models and Large Eddy Simulation (LES). The primary advantage of DES is that it can be applied at high Reynolds numbers as can Reynolds-averaged techniques, but also resolves geometry-dependent, unsteady three-dimensional turbulent motions as in LES. The initial applications of DES were favorable and formed the main motivation for developing the proposal that lead to initiation of the current Challenge project.

The compressible Navier-Stokes solver forming the backbone of this effort is Cobalt, a commercial version of the compressible flow solver Cobalt<sub>60</sub> developed at the Air Force Research Laboratory in support of the Common High Performance Software Support Initiative (CHSSI). The relevant improvements available in the commercial version and central to the success of the current project are flow-field computations of geometries undergoing rigid body motion, faster per-iteration times, the inclusion of SST-based DES, improved boundary layer tripping, ability to calculate time-averages and turbulence statistics, an improved spatial operator, and improved temporal integration. Strang *et al.* [2] validated the code on a number of problems, including the Spalart-Allmaras model (which forms the core of the DES model). Tomaro *et al.* [3] converted Cobalt<sub>60</sub> from explicit to implicit time integration, enabling CFL numbers as high as one million. Grismer *et al.* [4] then parallelized the code, yielding a linear speedup on as many as 1024 processors. Forsythe *et al.* [5] provided a comprehensive testing/validation of the RANS models. Parallel METIS domain decomposition library of Karypis and Kumar [6], Karypis *et al.* [7] is incorporated in Cobalt. ParMetis divides the grid into nearly equally sized zones that are then distributed one per processor.

This manuscript is a summary of the work accomplished under the current Challenge project. Due to the large scope of the project, only brief summaries of the various calculations that have been undertaken is provided, with references to more detailed treatments. A summary of the

perspectives developed during the course of this project is also provided.

## Computational Approach

### Spalart-Allmaras Model

The turbulence treatment in the majority of DES work to date is based on the Spalart-Allmaras (SA) one-equation RANS model [8]. In this model, a single partial differential equation is solved for a variable  $\tilde{\nu}$  which is related to the turbulent viscosity. The differential equation is derived by “using empiricism and arguments of dimensional analysis, Galilean invariance and selected dependence on the molecular viscosity.”[9] The model includes a wall destruction term that reduces the turbulent viscosity in the log layer and laminar sublayer and trip terms that provides a smooth transition from laminar to turbulent flow. As illustrated in the subsequent sections, the trip terms are important for some of the calculations in order to match conditions of particular experiments.

In the S-A RANS model, a transport equation is used to compute a working variable used to form the turbulent eddy viscosity,

$$\begin{aligned} \frac{D\tilde{\nu}}{Dt} &= c_{b1}[1 - f_{t2}]\tilde{S}\tilde{\nu} - \left[ c_{w1}f_w - \frac{c_{b1}}{\kappa^2}f_{t2} \right] \left[ \frac{\tilde{\nu}}{d} \right]^2 \\ &+ \frac{1}{\sigma} \left[ \nabla \cdot ((\nu + \tilde{\nu})\nabla\tilde{\nu}) + c_{b2}(\nabla\tilde{\nu})^2 \right] + f_{t1}\Delta U^2, \end{aligned} \quad (1)$$

where  $\tilde{\nu}$  is the working variable. The eddy viscosity  $\nu_t$  is obtained from,

$$\nu_t = \tilde{\nu} f_{v1}, \quad f_{v1} = \frac{\chi^3}{\chi^3 + c_{v1}^3}, \quad \chi \equiv \frac{\tilde{\nu}}{\nu}, \quad (2)$$

where  $\nu$  is the molecular viscosity. The production term is expressed as,

$$\tilde{S} \equiv f_{v3}S + \frac{\tilde{\nu}}{\kappa^2 d^2} f_{v2}, \quad f_{v2} = \left( 1 + \frac{\chi}{c_{v2}} \right)^{-3}, \quad f_{v3} = \frac{(1 + \chi f_{v1})(1 - f_{v2})}{\chi}, \quad (3)$$

where  $S$  is the magnitude of the vorticity. The production term as written in (3) differs from that developed in Spalart and Allmaras[8] via the introduction of  $f_{v3}$  and re-definition of  $f_{v2}$ . These changes do not alter predictions of fully turbulent flows and have the advantage that for simulation of flows with laminar separation, spurious upstream propagation of the eddy viscosity into attached, laminar regions is prevented. This modification was crucial for successful simulation of the flow around the forebody section summarized below. The function  $f_w$  is given by,

$$f_w = g \left[ \frac{1 + c_{w3}^6}{g^6 + c_{w3}^6} \right]^{1/6}, \quad g = r + c_{w2}(r^6 - r), \quad r \equiv \frac{\tilde{\nu}}{\tilde{S}\kappa^2 d^2}. \quad (4)$$

The function  $f_{t2}$  is defined as,

$$f_{t2} = c_{t3} \exp(-c_{t4}\chi^2). \quad (5)$$

The trip function  $f_{t1}$  is specified in terms of the distance  $d_t$  from the field point to the trip, the wall vorticity  $\omega_t$  at the trip, and  $\Delta U$  which is the difference between the velocity at the field point and that at the trip,

$$f_{t1} = c_{t1} g_t \exp \left( -c_{t2} \frac{\omega_t^2}{\Delta U^2} [d^2 + g_t^2 d_t^2] \right), \quad (6)$$

where  $g_t = \min(0.1, \Delta U / \omega_t \Delta x)$  and  $\Delta x$  is the grid spacing along the wall at the trip. The constants are  $c_{b1} = 0.1355$ ,  $\sigma = 2/3$ ,  $c_{b2} = 0.622$ ,  $\kappa = 0.41$ ,  $c_{w1} = c_{b1} / \kappa^2 + (1 + c_{b2}) / \sigma$ ,  $c_{w2} = 0.3$ ,  $c_{w3} = 2$ ,  $c_{v1} = 7.1$ ,  $c_{v2} = 5$ ,  $c_{t1} = 1$ ,  $c_{t2} = 2$ ,  $c_{t3} = 1.1$ , and  $c_{t4} = 2$ .

## Detached-Eddy Simulation

Most of the turbulent flows modeled in this project are computed using Detached-Eddy Simulation. The original DES formulation is based on a modification to the Spalart-Allmaras RANS model[8] such that the model reduces to its RANS formulation near solid surfaces and to a subgrid model away from the wall[1]. The basis is to attempt to take advantage of the usually adequate performance of RANS models in the thin shear layers where these models are calibrated and the power of LES for resolution of geometry-dependent and three-dimensional eddies in other regions. The DES formulation is obtained by replacing in the S-A model the distance to the nearest wall,  $d$ , by  $\tilde{d}$ , where  $\tilde{d}$  is defined as,

$$\tilde{d} \equiv \min(d, C_{DES} \Delta). \quad (7)$$

In Eqn. (7), for the computations performed in this project,  $\Delta$  is the largest distance between the cell center under consideration and the cell center of the neighbors (i.e., those cells sharing a face with the cell in question). In “natural” applications of DES, the wall-parallel grid spacings (e.g., streamwise and spanwise) are on the order of the boundary layer thickness and the S-A RANS model is retained throughout the boundary layer, i.e.,  $\tilde{d} = d$ . Consequently, prediction of boundary layer separation is determined in the ‘RANS mode’ of DES. Away from solid boundaries, the closure is a one-equation model for the SGS eddy viscosity. When the production and destruction terms of the model are balanced, the length scale  $\tilde{d} = C_{DES} \Delta$  in the LES region yields a Smagorinsky eddy viscosity  $\tilde{\nu} \propto S \Delta^2$ . Analogous to classical LES, the role of  $\Delta$  is to allow the energy cascade down to the grid size; roughly, it makes the pseudo-Kolmogorov length scale, based on the eddy viscosity, proportional to the grid spacing. The additional model constant  $C_{DES} = 0.65$  was set in homogeneous turbulence[10]. Strelets [11] introduced a DES model based on Menter’s Shear Stress Transport model[12] that has been included in Cobalt during the course of this project.

## Representative Results

Presented in this section is a brief synopsis of the various flows that have been computed over the course of the project. Important in application, assessment, and improvement of a technique for predicting turbulent flows such as Detached-Eddy Simulation is construction of an experience base that can be used to provide insight and knowledge useful for addressing potential problems and guiding the success of future efforts as the method is applied to new configurations and extended to new areas. Each of the flows summarized below possesses elements that have been valuable in advancing the computational approach and improving DES capabilities for engineering and scientific applications.

### Circular Cylinder

An important feature of DES is that prediction of boundary layer separation is accomplished using a RANS model, taking advantage of the reasonable range of flows for which the S-A model

yields adequate predictions. High Reynolds number flows experiencing turbulent boundary layer separation are out of reach of whole-domain LES since the boundary layer needs to be resolved, rather than modeled if the near-wall flow is computed. This becomes impractical for high Reynolds number flows and, consequently, DES offers strong advantages as an approach for high Reynolds number prediction. Figure 1 shows the flow over a section of a circular cylinder at a super-critical Reynolds number (separation of turbulent boundary layers). Boundary layer separation is delayed relative to sub-critical flows that experience laminar detachment. The separation prediction in Figure 1 is handled by the RANS (S-A) model. The shear layers that detach from the cylinder rapidly grow new instabilities and chaotic, three-dimensional structures quickly fill the wake.

## Rounded Square

One of the most significant factors affecting spin characteristics for modern fighters is the forebody, with its complex vortical flows and long moment arm. Laboratory measurements of spin characteristics are of limited utility since it is not possible to resolve important Reynolds number effects because of the range of available tunnels. A “building-block” flow considered as part of the current research is that around a canonical forebody cross section, the rounded-corner square. The flow visualization shown in Figure 2 illustrates the complex and highly three-dimensional structure in the wake. The Reynolds number of the calculation is high enough that whole-domain LES would be impractical. Squires *et al.* [13] have shown that the high Reynolds number DES predictions of the flow around the forebody are in good agreement with measurements, in contrast to both RANS and LES calculations.

## Delta Wing

The flow over a  $70^\circ$  delta wing has been computed at a Reynolds number of  $1.56 \times 10^6$  [14]. In this effort, a key finding was that the RANS region of DES was able to accurately predict the secondary separation, while the LES capability accurately resolved the windings that have been documented in experiments. Traditional RANS models, in contrast, were incapable of predicting the vortex breakdown. A comprehensive grid refinement study showed the capability of DES to predict finer scale turbulent structures as the grid resolution is increased.

Figure 3 depicts the flowfield solutions at the  $10,000^{th}$  time step for the coarse, medium, and fine grids. All three grid systems capture vortex breakdown, as well as the post-breakdown helical structures. The medium grid begins to show evidence of additional vortex structures winding around the primary vortex up to the breakdown position. The windings are even more evident in the fine grid. The breakdown position is also varying with grid density. The position moves slightly aft as grid is improved, thus becoming more in line with the experiment [15].

To determine the vortex core behavior with grid refinement, resolved turbulent kinetic energy (TKE) along the core was analyzed and is depicted in Figure 4. The maximum TKE in the core, nondimensionalized by the freestream velocity squared, increased from 0.17 for the coarse grid to 0.22 for the medium grid and 0.45 for the fine grid. The maximum TKE in the core was found in the experiments to be 0.5 [15].

## Supersonic Axisymmetric Base

Flow over the supersonic axisymmetric base of Herrin and Dutton [16] was predicted using DES and compared to LES and RANS results[17]. The effect of compressibility corrections and testing of SST based DES were key elements investigated in this work. Vorticity contours are presented in Figure 5, showing significant resolution of the turbulent structures in the wake. DES predictions exhibited substantial improvements over RANS models in the ability to predict both the overall base drag, and the flat pressure distribution on the base itself. DES predicted the correct boundary layer thickness prior to the base because of its RANS treatment. Whole-domain LES, on the other hand, was unable to adequately resolve the boundary layer, resulting in an under-prediction of its thickness. Off body Mach contours and turbulent statistics compared favorably with experiments.

## NACA 0012 Pitchup

A key goal of the present research is to develop an accurate and computationally feasible method for predicting aircraft spin. DES is formulated to provide accurate predictions of the massively separated flows characterizing a spin. Another important requirement in predicting spin is computation of an aircraft undergoing rigid body motion, a capability introduced into Cobalt during the course of this work. As a test of the new capability, the pitchup of two-dimensional NACA 0012 airfoil was computed for the same conditions as reported by Morgan and Visbal [18]. The calculation was at a Reynolds 12,600, no explicit turbulence model was used. The grid was provided by Morgan and Visbal [18], enabling a code-to-code comparison as validation for Cobalt. Vorticity contours are shown in Figure 6 during the pitch maneuver. Lift coefficient vs. angle-of-attack were virtually identical to the calculations of Morgan and Visbal [18]. Angles of the primary, secondary, and tertiary vortex formation also agreed well with the previous computations and the experiments of Gendrich [19].

## Prolate Spheroid

Flow over a prolate spheroid is a challenging test case for models. A complex separation develops over the body at incidence, the structure of the separated flow being sensitive to the angle of attack. Shown in Figure 7 is the surface distribution of the skin friction over the spheroid. The main experimental database for evaluation of DES predictions tripped the flow at  $x/L = 0.2$ . For the calculations, the trip terms summarized above in the S-A model are needed and activated at  $x/L = 0.2$  to produce the effect of transition to turbulence. The abrupt change in the skin friction pattern in the figure demonstrating this capability in the current computations.

## Forebody

In addition to the rounded-corner square summarized above, another forebody study has been undertaken. Unlike the rounded-corner square, the forebody shown in Figure 8 is three-dimensional, more closely approximating the forebody of an actual aircraft. Also motivating the particular configuration shown in the figure is the existence of rotary balance data for angles of attack of  $60^\circ$  and  $90^\circ$ . Shown in Figure 8 is a snapshot of the instantaneous flow at  $90^\circ$  angle of attack (flow from below to above in the figure). The flow visualization is from a computation at a Reynolds number based on the body width of  $2.1 \times 10^6$ . Time-dependent RANS (S-A) and DES predictions

are presented, each technique showing a relatively strong spanwise variation that would be impractical to resolve using whole-domain LES. Noteworthy is the more coherent structure on the nose of the forebody obtained in the RANS calculation (left frame of the figure). The surface pressure contours in the DES predictions show a more uniform distribution.

The different flow structures in the RANS and DES predictions of the forebody are apparent in the pressure coefficient distributions shown in Figure 9. The profiles are shown for the fourth measurement station from the tip, corresponding to the fourth plane in which eddy viscosity contours are drawn in Figure 8. The angle  $\theta$  is measured from the symmetry plane, beginning on the windward side. The distributions in the left frame are from computations of the static (non-rotating) flow, while those on the right are from preliminary simulations of the rotary flow at spin coefficient of 0.2. The pressure distributions for the static flow are essentially symmetric about  $\theta = 180^\circ$  for all the computations and the experimental measurements of Pauley *et al.* [20]. The minima in the vicinity  $\theta \approx 45^\circ$  and  $\theta \approx 315^\circ$  correspond to the windward front corners. Because the flow is fully turbulent at this Reynolds number, the boundary layers remain attached around the front corners, with separation occurring near  $\theta \approx 135^\circ$  and  $\theta \approx 225^\circ$ . The characteristically flat pressure distribution in the aft region ( $135^\circ < \theta < 225^\circ$ ) is accurately predicted in the DES. The RANS result, with its more coherent structure as evidenced in the surface pressures shown Figure 8, yields a pressure coefficient with substantially more variation than measured. These are important differences since RANS predictions of forces and moments are less accurate.

Shown in the right frame of Figure 9 is the forebody pressure distribution predicted in DES for a rotary motion of the forebody about the freestream velocity vector. Rotation is about the body center at a rate corresponding to a spin coefficient of 0.2. The asymmetry in the pressure distribution is apparent, with the region  $225^\circ < \theta < 315^\circ$  corresponding to the windward face of the forebody. The DES prediction in the figure adequately captures the attached flow around the lower front corner rotating into the flow ( $\theta \approx 315^\circ$ ), as well as the pressure variation on the leeward side. Current efforts are focusing on the role of grid refinement and comparison against RANS predictions.

## C-130

Airdrops are a major component of the ability of a country to project its forces around the world. Nevertheless, CFD is still rarely used to predict the airflow influence on airdrops due to the complexity of the problem. A greater understanding of the airflow in various airdrop configurations can both increase the safety of paratroopers and aircrews, and can aid future design and developmental testing of new airdrop configurations. The Challenge investigators are currently examining the safety of jumpmasters while performing door checks or the safety of towed jumpers in static line failures. The simulations performed will also serve to test the proper placement and sizing of extraction chutes in the wake of the aircraft. DES is used on the C-130H in order to predict the airflow in all the major airdrop configurations: gravity drop, extraction chute, and personnel drop. DES has also been used on the standard T-10 parachute in order to validate the computational approach on parachutes before studying the interactions between an extraction chute and the C-130.

Paratroopers whose chutes fail to deploy when static line jumping out of the cargo bay ramp of the C-130 can become entrained in the highly energetic separated flow characterizing this region and are often injured. Because of this problem, tailgate static lines are not employed. Using

CFD in concert with experiments to design an aircraft modification to circumvent this problem would enhance the capability of the C-130. A side-by-side water tunnel and CFD investigation was performed[22]. These initial calculations discovered the cause of the problem – two counter-rotating vortices are shed off the alternating sides of the cargo door, and create a large upward velocity in the plane of symmetry. This phenomenon prevents static line jumps off the cargo bay ramp. Currently static line jumps are performed out the side paratroop doors. This flow is currently being examined in order to observe the problems that could be encountered during door checks and during static line failures. The initial calculations presented in Figure 10 were made at 2° angle of attack at 140 KIAS at 500ft. This corresponds to a Reynolds number of approximately  $18 \times 10^6$ .

For cargo drops, commonly an extraction chute is used to pull the cargo out of the aft bay. Before mounting the extraction chute to the C-130 grid, the DES method was validated by studying the flow around a rigid non-porous canopy in an otherwise steady flow. These computations were made of a T-10 canopy, the standard U.S. Army chute, at a Reynolds number of  $4 \times 10^6$  corresponding to a steady descent of a 300lb load in an 18 ft/s descent. This chute has a nominal diameter of 35ft and an inflated diameter of 23.1ft. The resulting flow is pictured in Figure 11. Final results on all these calculations will be presented by the end of the year.

## **F-16**

The first DES calculation over an aircraft was made by Squires *et al.* [23] on the F-16 at 45° angle-of-attack. The grid consisted of  $3.1 \times 10^6$  cells for half the aircraft, with cells concentrated in the strake vortex. A comparison between DES and RANS was undertaken, shown in Figure 12. While unsteady RANS converged to a steady state solution, DES predicted a highly energetic turbulent flow. Strong pressure oscillations on the surface due to the vortex burst are apparent in Figure 13. Although there is no data to compare the vortex burst location, the delta wing studies of Morton *et al.* [14] lend credibility to these results. RANS calculations failed to predict a vortex burst, as also the case in the delta wing study. The success of this calculation on a relatively coarse grid (by LES standards) provided credible evidence that full aircraft calculations with DES were indeed practical. The calculation required 12.5 hours on 432 SP3 processors to compute 100 non-dimensional time units (made dimensionless using the chord and freestream velocity).

## **F/A-18E**

DES predictions were obtained of the flow around the F/A-18E to support the Abrupt Wing Stall program. Wind tunnel testing at transonic speeds revealed unsteady shock oscillations on the wing. Reynolds-averaged models appear to be incapable of predicting this unsteady oscillation. DES calculations have qualitatively produced the shock oscillation as shown in Figure 14 – showing two separate timesteps. The plane of x-vorticity behind the wing shows the fine scale structures captured by DES in this flow. More quantitative comparisons are underway with the aim of presenting results from that study next year.

## **F-15E**

Aircraft spin occurs at high angles of attack and in flows characterized by massive separation. The F-15E was selected for prediction of spin characteristics using DES since the aircraft underwent a

comprehensive flight-test spin program, and therefore provides an excellent validation case. DES and RANS calculations on the F-15E at  $65^\circ$  angle-of-attack have been performed by Forsythe *et al.* [24]. A timestep and grid sensitivity study comprised a key element of this work. The cells sizes of the meshes used for the grid sensitivity study were  $2.5 \times 10^6$ ,  $5.9 \times 10^6$ , and  $10.0 \times 10^6$ . Calculations were performed on as many as 256 processors, requiring about four days on the finest grid to obtain sufficient samples to represent the time-averaged flowfield. DES and RANS isosurfaces of vorticity are contrasted in Figure 15, with DES demonstrating an ability to predict the time-dependent and three-dimensional flow features characterizing the wake. The effect of grid refinement is shown in Figure 16. DES resolves additional finer-scale features as the grid density is increased. The (time-averaged) fine-grid DES lift, drag and pitching moment coefficients were within 5% of the flight-test data, with strong evidence of grid convergence.

## X-38

The full aircraft simulations detailed above as well as the fundamental flow predictions have built sufficient confidence in DES to encourage wider engineering use. The application of DES to the X-38 space station crew return vehicle represents such an application. Unsteady low frequency flow features were detected in flight test using unsteady pressure taps by NASA Dryden. Flow field asymmetries were also observed to cause a rolling moment. In an attempt to understand if these two phenomena were possibly related, a DES prediction was obtained at subsonic speeds. The flight test vehicle was laser scanned, providing the input geometry to the CFD calculation. The resulting flow is depicted in Figure 17. The unsteady separation occurring from the docking ring on top of the aircraft is a striking feature of the flow. Detailed analysis of these results is currently underway, and will be reported to NASA by the end of this year.

## Concluding Remarks

Work to date has provided key advances in application, assessment, and improvement of Detached-Eddy Simulation. Computation of building-block flows such as two- and three-dimensional forebodies and delta wings has established a foundation for resolution of several issues important to using DES to predict the flow field around full aircraft, helping to provide guidance in grid-generation aspects, turbulence treatments, and numerical parameters. The subsequent application of DES to the F-16 and F-15E has further enhanced our confidence level with lift and drag predictions that are accurate compared to flight test data. These developments will soon provide aircraft designers with a powerful tool for the prediction of massively separated flows over complex configurations and at flight conditions. The successful pressure predictions on the supersonic axisymmetric base reveals DES as capable of predicting missile afterbody flows. Successful calculations on the prolate spheroid could extend application of DES to maneuvering vehicles such as submarines. The availability of high performance computing and Challenge status continues to accelerate the development of this powerful technique.

DES applied today using HPC machines with massive processing capacity is making more “routine” the full-configuration prediction of complex geometries and at flight conditions. Accuracy in lift, drag, and moment predictions around the F-15E, for example, are within 5% of flight test data. These and other computations undertaken in the course of the current Challenge project are computed using  $\mathcal{O}(10 \times 10^6)$  mesh points. While already relatively accurate, increases in HPC

capacity will enable efficient simulation using substantially larger grids. DES flow fields will offer richer detail on denser grids, with associated increases anticipated in overall accuracy. Increases in HPC capacity coupled with the emergence of more efficient and accurate algorithms will soon enable prediction of additional physical effects such as fluid-structure interactions. An example of current interest being the aeroelastic properties of fighter aircraft in which the fluid flow is modeled using DES. In the longer term, aeroacoustic studies for aircraft will become possible and with sufficient capacity it is not unreasonable to believe that Computational Fluid Dynamics could be used to cover the entire flight envelope of an airplane on the timescales required by designers and engineers.

## Acknowledgments

The authors gratefully acknowledge the support of AFOSR Grant F49620-00-1-0050 (Program Manager: Dr. Tom Beutner) and F49620-02-1-0117 (Program Managers: Dr. Tom Beutner and Dr. John Schmisser). The authors are also grateful for the assistance of Dr. Glen Peters, Dr. Ken Walck, and Dr. Walt Labozzetta of Boeing Military, who provided the stability and control database and the F-15E geometry. Mr. Matthieu Chapelet, Cadet Kory Klismith, and Mr. Aroon Viswanathan have assisted with grid generation and post-processing. Cadet Warren Carroll and Cadet Alan Vant-Land aided in post-processing the F-15E results. Finally, the project would not have been possible without the support and cpu hours at Maui HPCC and NAVO MSRC.

## References

- [1] Spalart, P. R. , Jou W-H. , Strelets M. , and Allmaras, S. R., “Comments on the Feasibility of LES for Wings, and on a Hybrid RANS/LES Approach,” *Advances in DNS/LES, 1st AFOSR Int. Conf. on DNS/LES*, Aug 4-8, 1997, Greyden Press, Columbus Oh.
- [2] Strang, W. Z., Tomaro, R. F, Grismer, M. J., “The Defining Methods of Cobalt<sub>60</sub>: a Parallel, Implicit, Unstructured Euler/Navier-Stokes Flow Solver,” *AIAA 99-0786*, January 1999.
- [3] Tomaro, R.F., Strang, W. Z., and Sankar, L. N., “An Implicit Algorithm for Solving Time Dependent Flows on Unstructured Grids,” *AIAA 97-0333*, January 1997.
- [4] Grismer, M. J., Strang, W. Z., Tomaro, R. F. and Witzemman, F. C., “Cobalt: A Parallel, Implicit, Unstructured Euler/Navier-Stokes Solver,” *Advances in Engineering Software*, Vol. 29, No. 3-6, pp. 365—373, 1998.
- [5] Forsythe, J.R., Strang, W., Hoffmann, K.A., “Validation of Several Reynolds-Averaged Turbulence Models in a 3D Unstructured Grid Code,” *AIAA 00-2552*, June 2000.
- [6] Karypis, G., and Kumar, V., *METIS: Unstructured Graph Partitioning and Sparse Matrix Ordering System Version 2.0*. University of Minnesota, Department of Computer Science, Minneapolis, MN 55455, July 1997.
- [7] Karypis, G., Schloegel, K., and Kumar, V, *ParMETIS: Parallel Graph Partitioning and Sparse Matrix Ordering Library Version 1.0*. University of Minnesota, Department of Computer Science, Minneapolis, MN 55455, July 1997.

- [8] Spalart, P.R. and Allmaras, S.R., 1994, "A One-Equation Turbulence Model for Aerodynamic Flows," *La Recherche Aerospatiale* **1**, pp. 5-21.
- [9] Spalart, P. R., "Strategies for Turbulence Modeling and Simulations," 4th Int. Symp. Eng. Turb. Modelling and Measurements, Corsica, May 24-26, 1999.
- [10] Shur, M., Spalart, P. R., Strelets, M., and Travin, A., "Detached-Eddy Simulation of an Airfoil at High Angle of Attack, 4th Int. Symp. Eng. Turb. Modelling and Measurements, Corsica, May 24-26, 1999.
- [11] Strelets, M., "Detached Eddy Simulation of Massively Separated Flows", *AIAA 01-0879*, Jan 2001.
- [12] Menter, F.R., "Improved Two-Equation  $k-\omega$  Turbulence Models for Aerodynamic Flows," *NASA-TM-103975*, October 1992.
- [13] Squires, K.D., Forsythe, J.R. and Spalart, P.R., "Detached-Eddy Simulation of the separated flow around a forebody cross-section", *Direct and Large-Eddy Simulation IV*, ERCOFTAC Series – Volume 8, B.J. Geurts, R. Friedrich and O. Metais, editors, Kluwer Academic Press, pp. 481-500, 2001.
- [14] Morton, S. A., Forsythe, J. R., Mitchell, A. T., Hajek, D., "DES and RANS Simulations of Delta Wing Vortical Flows", *AIAA 02-0587*, January 2002.
- [15] Mitchell, A.M., Molton, P., Barberis, D., Delery, J., "Oscillation of Vortex Breakdown Location and Control of the Time-Averaged Location by Blowing," *AIAA Journal*, V. 38, No. 5, May 2000, pp. 793-803.
- [16] Herrin, J. L., Dutton, J. C., "Supersonic Base Flow Experiments in the Near Wake of a Cylindrical Afterbody," *AIAA Journal*, Vol. 32, No1, Jan 1994.
- [17] Forsythe, J. R., Hoffmann, K. A., Squires, K. D., "Detached-Eddy Simulation with Compressibility Corrections Applied to a Supersonic Axisymmetric Base Flow", *AIAA 02-586*, January 2002.
- [18] Morgan, P. E., Visbal, M. R., "Simulation of Unsteady Three-dimensional Separation on a Pitching Wing", *AIAA 01-2719*, June 2001.
- [19] Gendrich, C., *Dynamic Stall of Rapidly Pitching Airfoils: MTV experiments and Navier-Stokes Simulation*, Ph.D. thesis, Michigan State University, 1999.
- [20] Pauley, H., Ralston, J. and Dickes, E., "Experimental study of the effects of Reynolds number on high angle of attack aerodynamic characteristics of forebodies during rotary motion", NASA Contractor Report 195033, January 1995.
- [21] Storms, B. L., Ross, J. C., Heineck, J. T., Walker, S. M., Driver, D. M., Zilliac, G. G., "An Experimental Study of the Ground Transportation System (GTS) Model in the NASA Ames 7- by 10-Ft Wind Tunnel," *NASA TM*.

- [22] Johnson, W., Trickey, C., Forsythe, J., Albertson, J., Leigh, E., “Experimental and Computational Investigation of the Flow Behind a C-130 with Tailgate Down,” *AIAA 02-0713*, January 2002.
- [23] Squires, K. D., Forsythe, J. R., Wurtzler, K. E., Strang, W. Z., Tomaro, R. F., Grismer, M. J., and Spalart, P. R., “Towards Prediction of Aircraft Spin,” *High Performance Computing Users Group Meeting, 2001*, July 2001.
- [24] Forsythe, J. R., Squires, K. D., Wurtzler, K. E., Spalart, P. R., “Detached-Eddy Simulation of Fighter Aircraft at High Alpha,” *AIAA 02-0591*, January 2002.

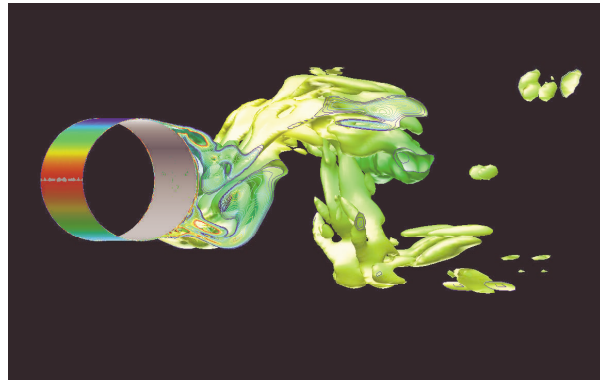


Figure 1: DES prediction of the flow over a circular cylinder at  $Re = 800,000$ . Isosurface of vorticity colored by pressure shown for a single realization.

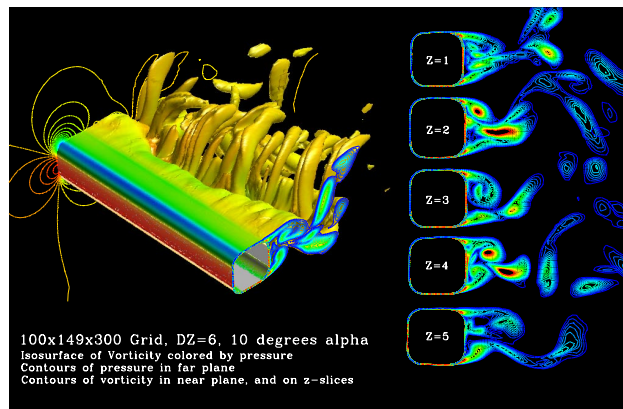


Figure 2: DES prediction of the flow over a rounded-corner square at  $Re = 800,000$ . Isosurface of vorticity colored by pressure shown for a single realization in the perspective view. Vorticity contours are shown in five planes along the span for the same instant in time.

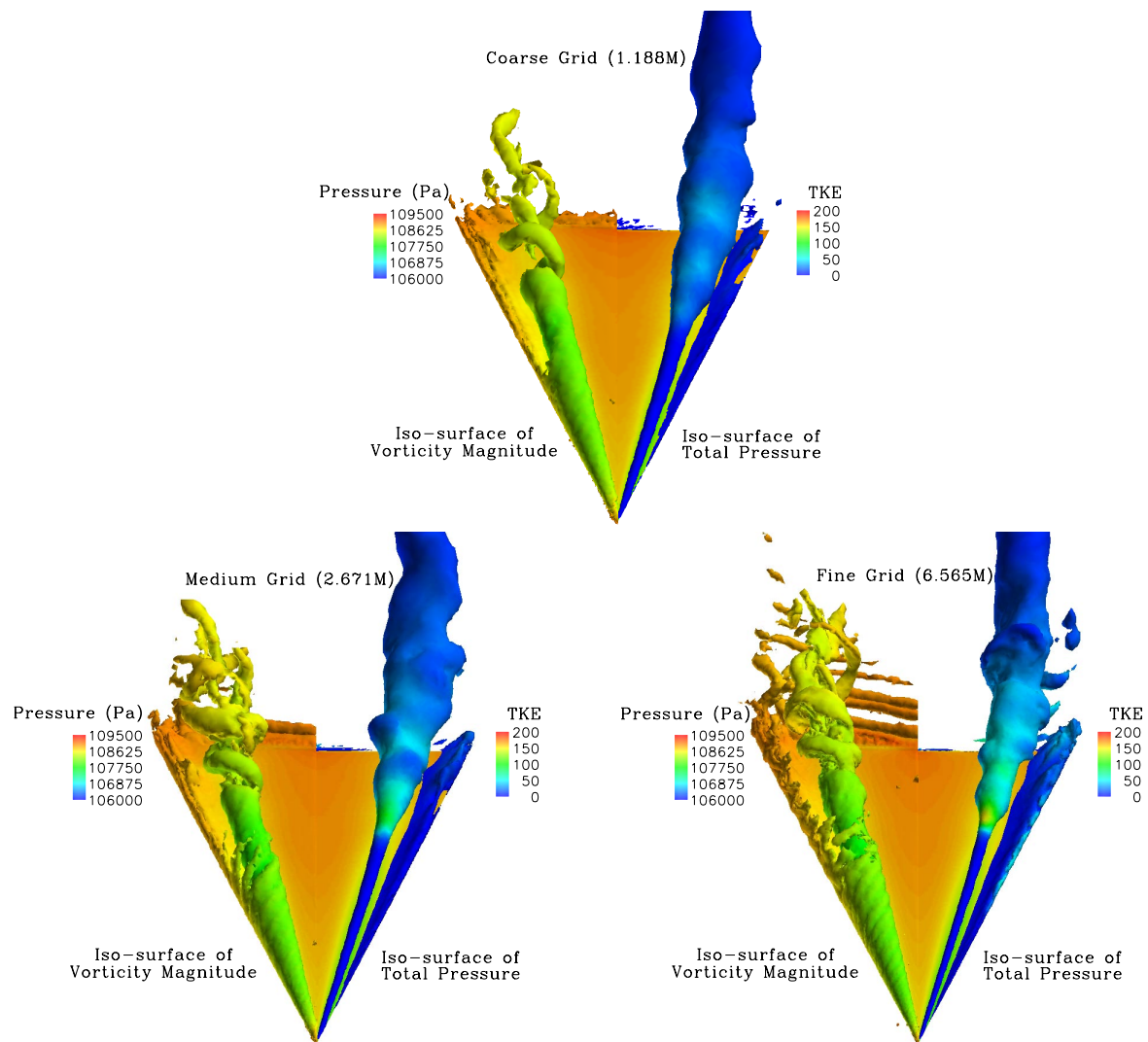


Figure 3: Flowfield solutions for three grids containing iso-surfaces of vorticity magnitude and total pressure.

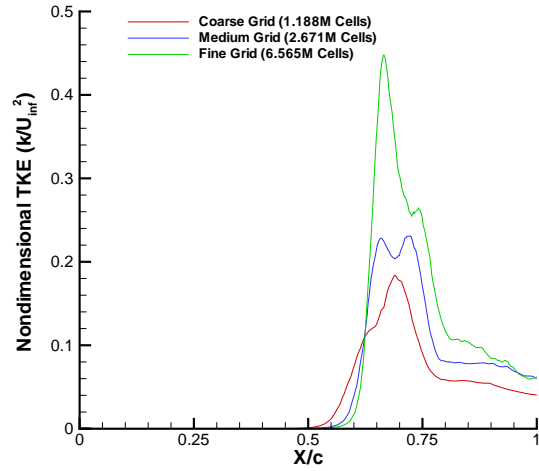


Figure 4: Resolved turbulent kinetic energy along the core of the vortex.

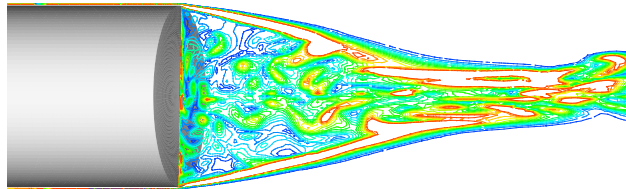


Figure 5: DES prediction of flow over an axisymmetric base at Mach 2.46. Vorticity contours from a single realization shown in the wake.

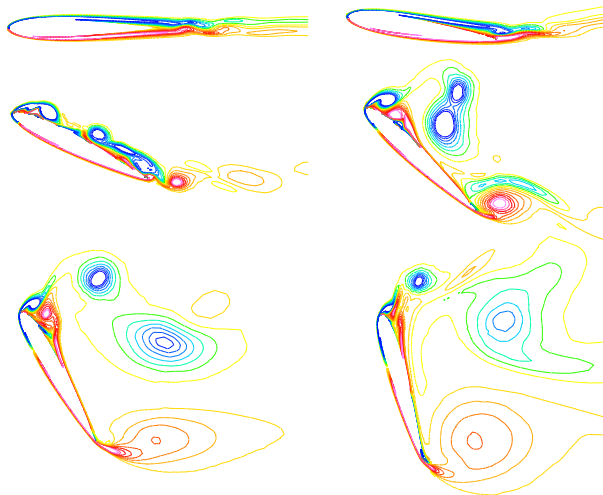


Figure 6: Vorticity contours in the wake at six phases in the unsteady pitchup of a NACA 0012 airfoil.

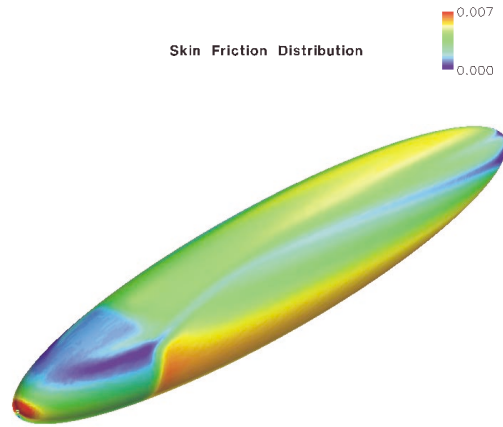


Figure 7: DES prediction of the flow over a prolate spheroid. Skin friction contours shown for the flow at  $20^\circ$  angle of attack.

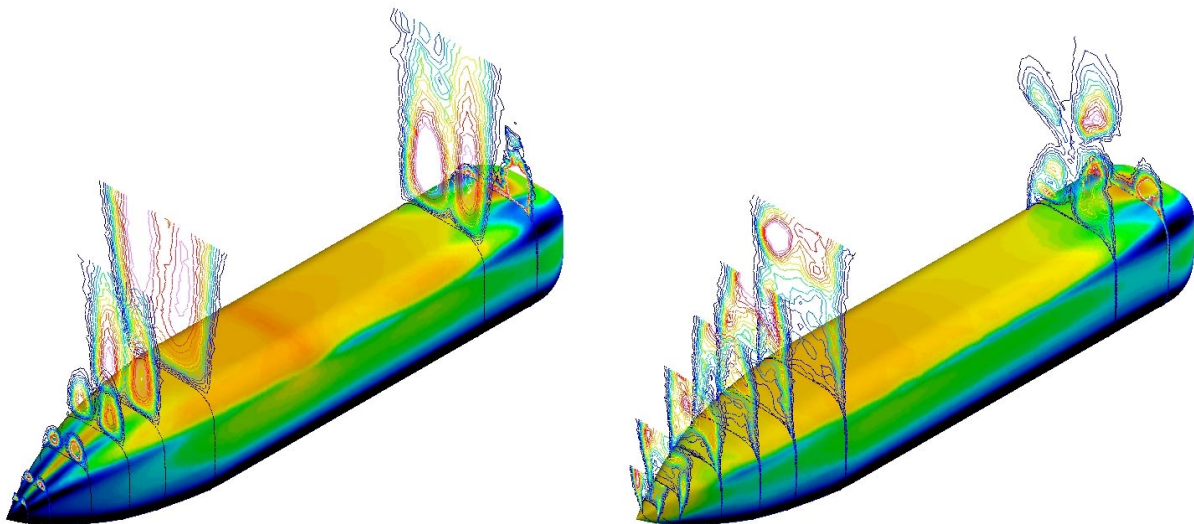


Figure 8: DES (right frame) and RANS (left frame) predictions of flow over a three-dimensional forebody at  $90^\circ$  angle-of-attack. Eddy viscosity contours from a single realization at the eight axial stations for which experimental measurements of the pressure distribution are available. The instantaneous pressure distribution is shown on the forebody surface.

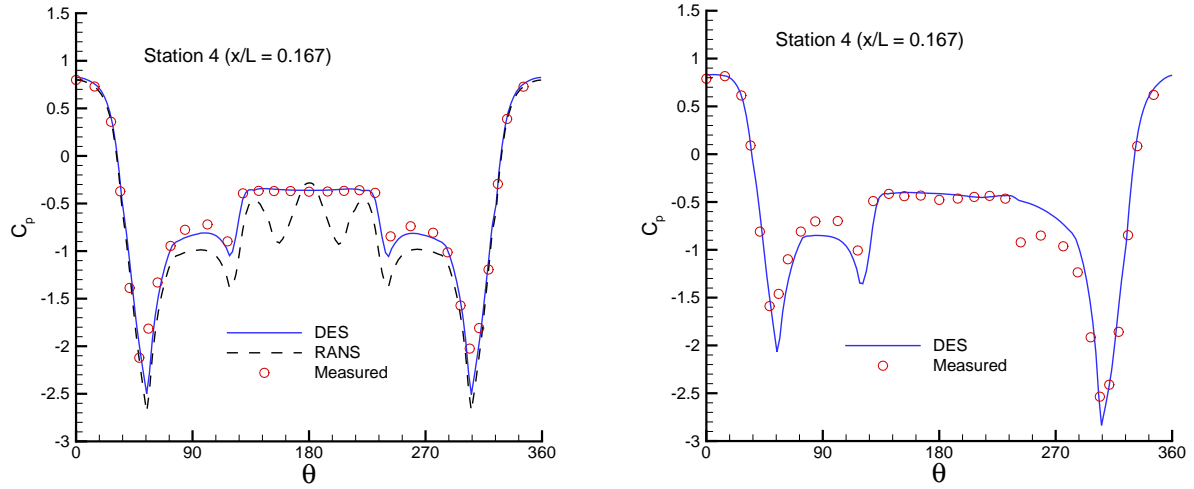


Figure 9: DES and RANS predictions of the time-averaged pressure coefficient around the forebody shown in Figure 8. Shown on the left are  $C_p$  predictions for the static flow from RANS and DES, shown on the right are the  $C_p$  predictions of the flow with rotary motion (about the freestream velocity vector). Measurements are from Pauley *et al.*(1995).



Figure 10: DES prediction of flow over the C-130H with paratroop doors open. Isosurface of vorticity colored by pressure.

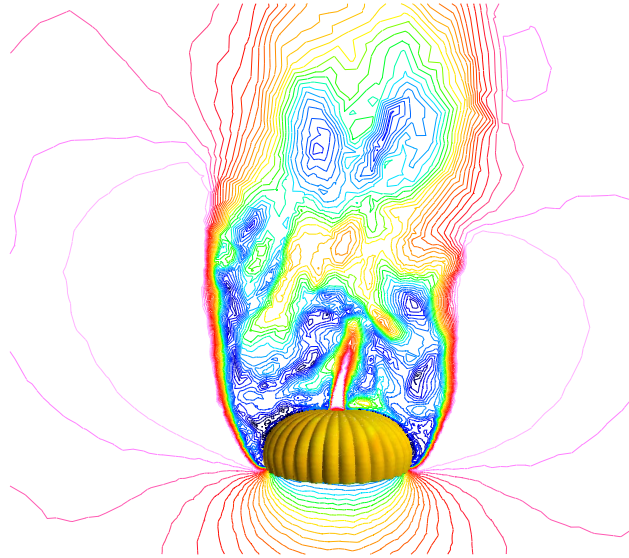


Figure 11: Contours of the velocity magnitude from DES predictions of the T-10 parachute.

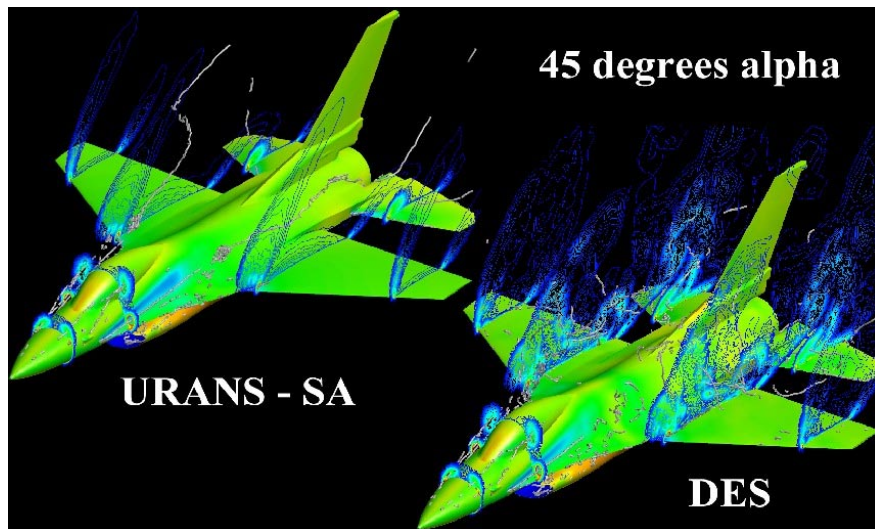


Figure 12: DES predictions of the flow over the F-16 at  $45^\circ$  angle-of-attack – DES vs. Unsteady RANS. The surface is colored by pressure, contours are of vorticity, and gray filaments are auto-detected vortex cores.

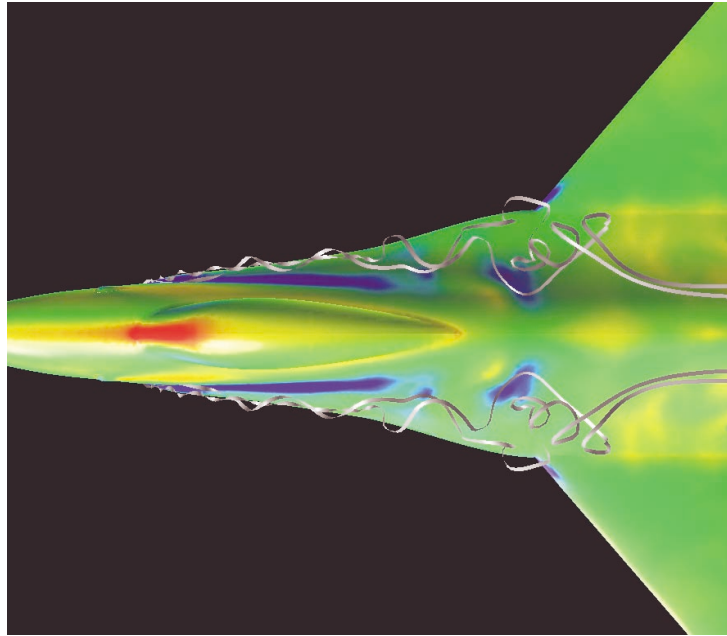


Figure 13: DES prediction of flow over the F-16 at  $45^\circ$  angle-of-attack – surface colored by pressure, and streamlines.

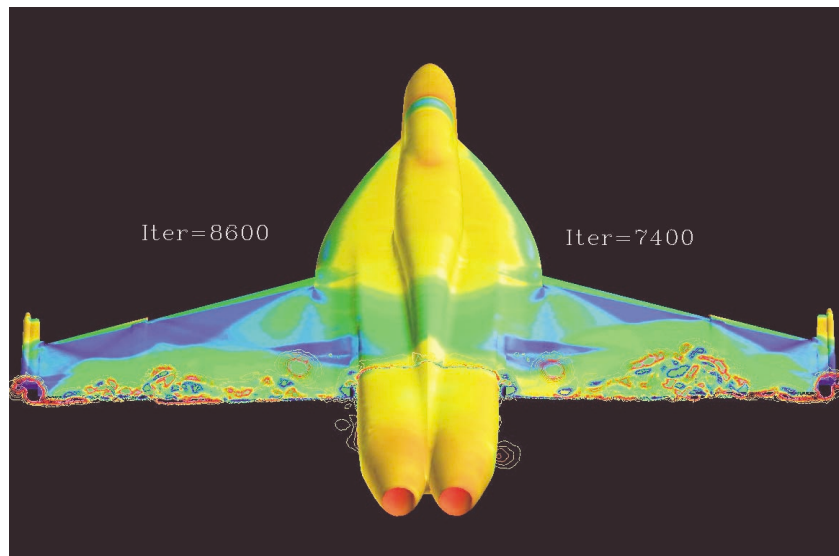


Figure 14: DES prediction of flow over the F/A-18E – surface colored by pressure and contours of vorticity.

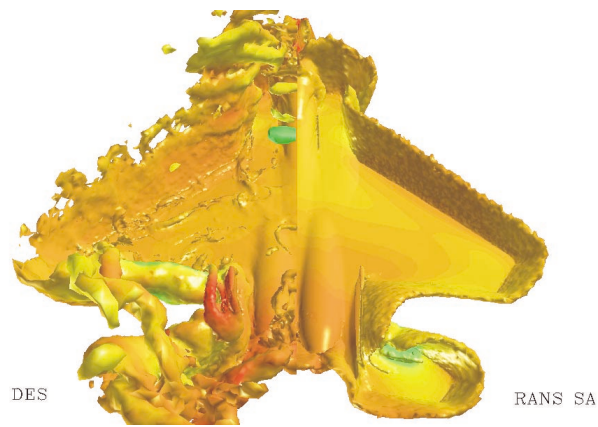


Figure 15: DES prediction of flow over the F-15E at 65° angle-of-attack – DES vs. RANS. Isosurface of vorticity colored by pressure.

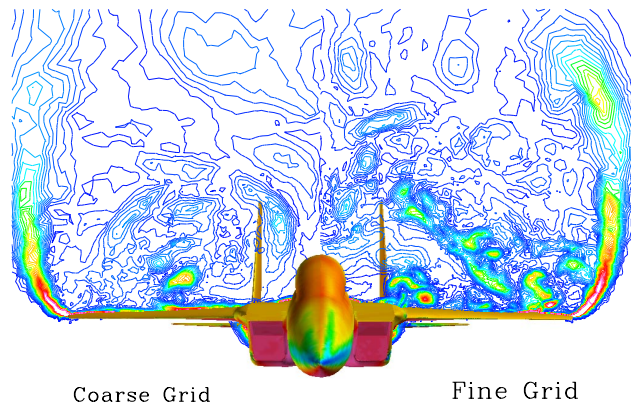


Figure 16: Instantaneous vorticity contours at 680 inches behind the aircraft reference point. Coarse-grid prediction in left-half plane, fine-grid result in right-half plane.

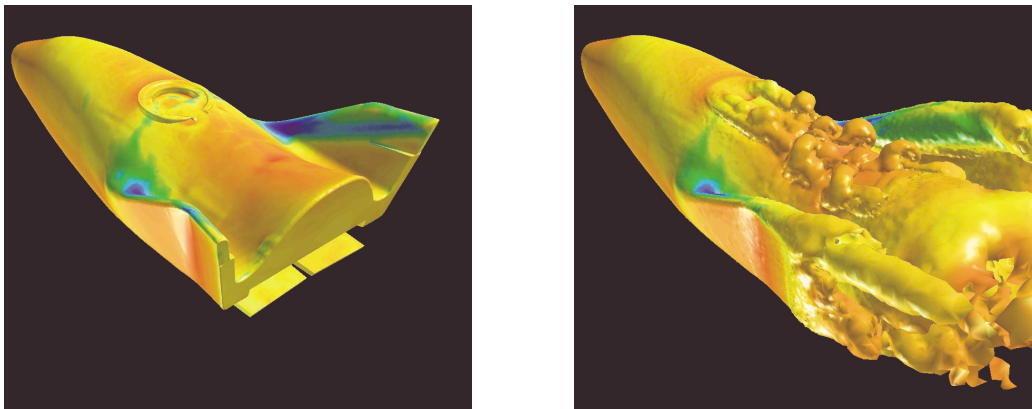


Figure 17: DES prediction of flow over the X-38 crew return vehicle. Vehicle is shown with and without isosurface of vorticity. Vehicle and isosurface is colored by pressure.